International Journal of Applied Mechanics
Vol. 1, No. 1 (2009) 233–258

ICP Imperial College Press
www.icpress.co.uk

A NOVEL SCHEME OF STRAIN-CONSTRUCTED POINT INTERPOLATION METHOD FOR STATIC AND DYNAMIC MECHANICS PROBLEMS

G. R. LIU*,† and G. Y. ZHANG†,‡

*Centre for Advanced Computations in Engineering Science (ACES)
Department of Mechanical Engineering
National University of Singapore (NUS)
9 Engineering Drive 1, 117576, Singapore

†Singapore-MIT Alliance (SMA), E4-04-10
4 Engineering Drive 3, 117576, Singapore

Received 12 February 2009
Accepted 23 February 2009

This paper presents a new scheme of strain-constructed point interpolation method (SC-PIM) for static, free and forced vibration analysis of solids and structures using triangular cells. In the present scheme, displacement fields are assumed using shape functions created via the point interpolation method (PIM), which possess the Kronecker delta property facilitating the straightforward enforcement of displacement boundary conditions. Using the generalized gradient smoothing technique, the "smoothed" strains at the middle points of the cells edges are first obtained using the corresponding edge-based smoothing domains and the assumed displacement field. In each triangular background cell, the strains at the vertices are assigned using these smoothed strains in a proper manner, and then piecewisely linear strain fields are constructed by the linear interpolation for each sub-triangular cell using the edge-based "smoothed" strains. With the assumed displacements and constructed linear strain fields, the discretized system equations are created using the Strain Constructed Galerkin (SC-Galerkin) weak form. A number of benchmark numerical examples, including the standard patch test, static, free and forced vibration problems, have been studied and intensive numerical results have demonstrated that the present method possesses the following properties: (1) it works well with the simplest triangular mesh, no additional degrees of freedom and parameters are introduced and very easy to implement; (2) it is at least linearly conforming; (3) it possesses a close-to-exact stiffness: it is much stiffer than the "overly-soft" node-based smoothed point interpolation method (NS-PIM) and much softer than the "overly-stiff" FEM model; (4) the results of the present method are of superconvergence and ultra-accuracy: about one order of magnitude more accurate than those of the linear FEM; (5) there are no spurious non-zeros energy modes found and it is also temporally stable, hence the present method works well for dynamic problems.

Keywords: Numerical method; meshfree method; point interpolation method; weakened weak form; gradient smoothing; strain construction.

‡Corresponding author: Guiyong Zhang, Center for Advanced Computations in Engineering Science (ACES), Department of Mechanical Engineering, National University of Singapore, 9 Engineering Drive 1, 117576, Singapore. Tel.: +65-65164796; Email: guiyong@gmail.com

1. Introduction

As one of the most powerful numerical methods used for simulation of physical phenomena, the finite element method (FEM) has been well developed and applied to different types of practical engineering problems with various commercial software package available (Zienkiewicz and Taylor, 2000; Liu and Quek, 2003). However, FEM has some intrinsic features which limit the application to some problems. One example is the well-known "overly-stiff" phenomenon, which is involved in a fully-compatible FEM model of assumed displacement based on the standard Galerkin weak form, and may cause the following problems: (1) the so-called "locking" behavior for many problems, (2) inaccuracy in stress solutions, and (3) poor solution using linear triangular mesh.

Many efforts have been made to solve the overly-stiff problem involved in a fully compatible FEM model, such as the development of hybrid FEM formulations (Pian and Wu, 2006). Using the generalized gradient smoothing technique, Liu and coworkers have developed a series of novel numerical methods, which can effectively soften the stiffness of the model and hence make these methods possess a number of attractive features (Liu, 2008a; b). In the scheme of meshfree methods, the node-based smoothed point interpolation method (NS-PIM)[a] has been proposed using the generalized node-based strain smoothing technique (Liu and Zhang *et al.*, 2005; Zhang and Liu *et al.*, 2007). In the NS-PIM, the displacement field is approximated using the PIM (polynomial PIM or radial PIM) shape functions, which possess the Kronecker delta property for easy treatment of essential boundary conditions. Different from the traditional FEM, the strains in the NS-PIM are obtained using the generalized smoothing technique (Liu, 2008a) that were extended from the strain smoothing technique (Chen *et al.*, 2001), and the discretized system equations are derived using the generalized smoothed Galerkin (GS-Galerkin) weak form which allows the use of discontinuous functions (Liu, 2008a). It was found that the NS-PIM is at least linearly conforming, can provide much better stress solutions, much more tolerant to mesh distortion, immune from the volumetric locking problem, works very well for linear triangular cells, and more importantly it can provide upper bound solution in energy norm with respect to both FEM and exact solutions (Liu and Zhang, 2008a). Thus using the NS-PIM together with the FEM, which provides lower bounds solutions, we have a systematical way to numerically obtain both upper and lower bounds of the exact solution (Zhang, Liu and Li, 2008). By extending the idea of NS-PIM to the FEM scheme, a node-based smoothed finite element method (NS-FEM) has been developed (Liu and Nguyen *et al.*, 2008). The NS-FEM can be viewed as the special case of NS-PIM using linear PIM shape functions and possesses similar properties as NS-PIM. It was found that both NS-PIM and NS-FEM are "overly-soft" and encounter the temporal instability problem when used to solve dynamic problems. Thus the very effective edge-based smoothed finite element

[a]The NS-PIM was originally termed as the linearly conforming point interpolation method (LC-PIM).

method (ES-FEM) has been proposed for 2D and 3D problems (Liu, Nguyen and Lam, 2008; Nguyen and Liu *et al.*, 2008), using the edge-based smoothing domains. Extending the idea of ES-FEM to the scheme of meshfree methods, the edge-based point interpolation method (ES-PIM) has been formulated with the presentation of cell-based T-schemes which are used to select the supporting nodes for the field variable approximation (Liu and Zhang, 2008b). Both ES-FEM and ES-PIM can produce vary accurate solutions, are temporally stable and hence work well for dynamic problems. In addition, cell-based smoothed methods have also formulated in the FEM settings known as the SFEM (Liu and Dai *et al.*, 2007; Liu and Trung *et al.* 2007) and in meshfree settings known as the CS-PIM (Liu and Zhang, 2009). All these models are at least better and many of them are much better than standard FEM.

In the above-mentioned PIMs, the smoothed strains are constant within each smoothing domain and hence the strain field is not continuous over the whole problem domain. By carefully reconstructing the strain fields, Liu and coworkers have developed a class of strain-constructed point interpolation methods (SC-PIM) (Liu and Zhang, 2008c). Different from the methods mentioned above, linear strain fields are constructed in the SC-PIM using the simple linear interpolation operation based on the smoothed and compatible strains and an SC-Galerkin weak form (extended Galerkin weak form) is used to drive the discretized system equations (Liu and Xu *et al.*, 2008). The SC-PIM models so constructed have a number of good properties, such as high accuracy, super convergence and upper bound solutions.

This paper presents a new scheme of SC-PIM. In the present scheme, the problem domain is discretized using the simple three-node triangular cells and the displacement field is constructed using the PIM shape functions that may not be continuous. Using the "smoothed" strains associated with the edges, strains at the vertices of the triangular cells in a proper manner, and linear strain fields are then formed using the simple linear interpolation over each sub-triangular cell, which is also serving as the integration cell, and the discretized system equations are finally formulated using the SC-Galerkin weak form. The method proposed will be used to study the static, free and forced vibration analysis of solid mechanics problems.

2. Brief on Basic Equations

Consider a two-dimensional static elasticity problem governed by the following equation in a physical domain Ω bounded by Γ ($\Gamma = \Gamma_u + \Gamma_t; \Gamma_u \cap \Gamma_t = 0$; Γ_u and Γ_t represent essential and natural boundaries respectively) as follow

$$\mathbf{L}_d^T \boldsymbol{\sigma} + \mathbf{b} = 0 \quad \text{in } \Omega \tag{2.1}$$

where $\mathbf{L}_d$ is a matrix of differential operator defined as

$$\mathbf{L}_d = \begin{bmatrix} \frac{\partial}{\partial x} & 0 \\ 0 & \frac{\partial}{\partial y} \\ \frac{\partial}{\partial y} & \frac{\partial}{\partial x} \end{bmatrix} \tag{2.2}$$

In Eq. (2.1), $\boldsymbol{\sigma}^T = \{\sigma_{xx} \;\; \sigma_{yy} \;\; \tau_{xy}\}$ is the stress vector, $\mathbf{b}^T = \{b_x \;\; b_y\}$ is the body force vector. The stresses are related to the strains via the generalized Hook's law:

$$\boldsymbol{\sigma} = \mathbf{D}\boldsymbol{\varepsilon} \tag{2.3}$$

where $\mathbf{D}$ is the matrix of material constants defined as follows:

$$\begin{aligned} \mathbf{D} &= \frac{E}{1-v^2}\begin{bmatrix} 1 & v & 0 \\ v & 1 & 0 \\ 0 & 0 & \frac{1-v}{2} \end{bmatrix} \quad \text{Plane stress} \\ \mathbf{D} &= \frac{E(1-v)}{(1+v)(1-2v)}\begin{bmatrix} 1 & \frac{v}{1-v} & 0 \\ \frac{v}{1-v} & 1 & 0 \\ 0 & 0 & \frac{1-2v}{2(1-v)} \end{bmatrix} \quad \text{Plane strain} \end{aligned} \tag{2.4}$$

In Eq. (2.3), $\boldsymbol{\varepsilon}^T = \{\varepsilon_{xx} \quad \varepsilon_{yy} \quad 2\varepsilon_{xy}\} = \{\varepsilon_{xx} \quad \varepsilon_{yy} \quad \gamma_{xy}\}$ is the vector of strains, which relate to the displacements by the following compatibility equation:

$$\boldsymbol{\varepsilon} = \mathbf{L}_d\mathbf{u} \tag{2.5}$$

where $\mathbf{u} = \{u_x \quad u_y\}^T$ is the displacement vector. The strains obtained using Eq. (2.5) are generally called compatible strains.

There are two types of boundary conditions, Dirichlet (or essential/displacement) boundary conditions and Neumann (or natural/stress) boundary conditions.

Dirichlet boundary conditions:

$$\mathbf{u} = \mathbf{u}_\Gamma \quad \text{on } \Gamma_u \tag{2.6}$$

where $\mathbf{u}_\Gamma$ is the vector of the prescribed displacements on the essential boundary Γ_u.

Neumann boundary conditions:

$$\mathbf{L}_n^T\boldsymbol{\sigma} = \mathbf{t}_\Gamma \quad \text{on } \Gamma_t \tag{2.7}$$

where $\mathbf{t}_\Gamma$ is the vector of the prescribed traction on the natural boundary Γ_t, and $\mathbf{L}_n$ is the matrix of unit outward normal which can be expressed as

$$\mathbf{L}_n = \begin{bmatrix} n_x & 0 \\ 0 & n_y \\ n_y & n_x \end{bmatrix} \tag{2.8}$$

in which n_x and n_y are unit outward normal in x and y directions respectively.

3. Formulations

3.1. *Displacements approximation using PIM*

For the present method, the displacement fields are constructed locally using the point interpolation method (PIM) with a small set of local nodes which are selected using the cell-based T-scheme (Liu and Zhang, 2008b). In detail, linear displace-

ments are constructed using PIM with the T3 scheme, which uses the three vertexes of a triangular cell to perform the interpolation and is exactly the same as the linear FEM. To obtain quadratic displacement fields, we use T6/3 scheme in which six and three nodes are selected for the interpolation of point of interest located in interior and boundary cells respectively. The detailed procedure of constructing PIM shape functions can be found in the meshfree book by Liu (2009). Using polynomial PIM shape functions, a displacement function u can then be expressed as

$$u(\mathbf{x}) = \sum_{i \in S_e} \phi_i(\mathbf{x}) d_i \tag{3.1}$$

where $\mathbf{x} = \{x \ \ y\}^T$, S_e is the set of the nodes in the local support domain that hosts the point of interest $\mathbf{x}$, d_i is a nodal displacement value, and ϕ_i is the PIM shape function which possesses the property of Kronecker delta: $\phi_i(\mathbf{x}_j) = \delta_{ij}(x, y)$ at node i, and evaluated at coordinates $\mathbf{x}_j$.

3.2. *Edge-based smoothed strains*

In the framework of W^2 formulation considering the possible discontinuous displacements field, the "smoothed" strains $\bar{\boldsymbol{\varepsilon}}_k$ are defined as (Liu, 2008b):

$$\bar{\boldsymbol{\varepsilon}}_k \equiv \frac{1}{A_k} \int_{\Gamma_k} \mathbf{L}_n \mathbf{u}(\mathbf{x}_k) d\Gamma \tag{3.2}$$

where Ω_k is a smoothing domain associated with the point of interest $\mathbf{x}_k$, $A_k = \int_{\Omega_k} d\Omega$ is the area of the smoothing domain associated with $\mathbf{x}_k$, and Γ_k is the boundary of the smoothing domain Ω_k. Note in Equation (3.2), we do not use the "compatible strains" because they may not exist at location in Ω_k need $\mathbf{u}$ only being integrable on Γ_k. Therefore, the "smoothed" strain $\bar{\boldsymbol{\varepsilon}}_k$ is not exactly the strain obtained by smoothing the compatible strain. It is, in fact, an approximated strain by "boundary flux equivalence".

For Equation (3.2) to work, the problem domain is discretized into N_s non-overlapping smoothing domains, as shown in (a) of Fig. 1, such that $\Omega = \Omega_1 \cup \Omega_2 \cup \cdots \cup \Omega_{N_s}$ and $\Omega_i \cap \Omega_j = \emptyset$, $i \neq j$, by which we require Γ_k does not share any finite portion of line segments where the PIM shape function is discontinuous. As a typical case, the edge-based smoothing domains are constructed with respect to the edges of the triangular background cells by connecting two ends of each edge to the centroids of two adjacent elements, as illustrated in (b) of Fig. 1. Thus the number of the smoothing domains (N_s) equals the number of edges of triangles (N_{edge}).

By substituting Equation (3.1) into Equation (3.2), the smoothed strain can be written in the following matrix form of nodal displacements:

$$\bar{\boldsymbol{\varepsilon}}_k = \frac{1}{A_k} \int_{\Gamma_k} \mathbf{L}_n \boldsymbol{\Phi} \boldsymbol{d}_i d\Gamma = \sum_{i \in N_{infl}} \bar{\mathbf{B}}_i(\mathbf{x}_k) \mathbf{d}_i \tag{3.3}$$

where $\boldsymbol{\Phi}$ is the matrix of PIM shape functions and N_{infl} is the number of field nodes involved in constructing the smoothed strain fields within Ω_k. When linear shape

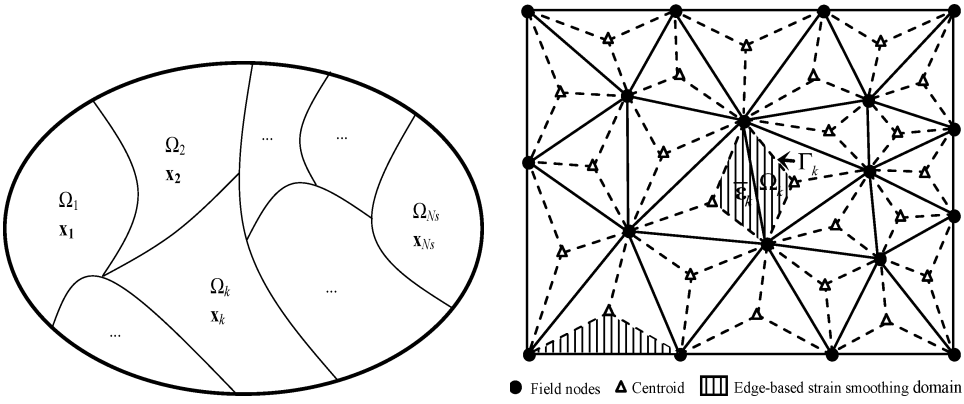

(a) General construction of stationary and non-overlapping smoothing domains

(b) Construction of edge-based smoothing domains based on three-node triangular background cells

Fig. 1. Illustration of the construction of stationary and non-overlapping smoothing domains.

functions are used, N_{infl} equals exactly the number of nodes whose host triangular cells are involved in the strain smoothing upon Ω_k. In Equation (3.3), $\bar{\mathbf{B}}_i(\mathbf{x}_k)$ is termed as the smoothed strain matrix that can be expressed as

$$\bar{\mathbf{B}}_i(\mathbf{x}_k) = \begin{bmatrix} \bar{b}_{ix}(\mathbf{x}_k) & 0 \\ 0 & \bar{b}_{iy}(\mathbf{x}_k) \\ \bar{b}_{iy}(\mathbf{x}_k) & \bar{b}_{ix}(\mathbf{x}_k) \end{bmatrix} \tag{3.4}$$

In the above equation, elements of the smoothed strain matrix can be calculated as

$$\bar{b}_{il}(\mathbf{x}_k) = \frac{1}{A_k} \int_{\Gamma_k} \varphi_i(\mathbf{x}_k) n_l(\mathbf{x}_k) d\Gamma \quad (l = x, y) \tag{3.5}$$

Using Gauss integration scheme, the above integration can be further obtained as follows:

$$\bar{b}_{il} = \frac{1}{A_k} \sum_{m=1}^{N_{seg}} \left[\sum_{n=1}^{N_{gau}} w_n \varphi_i(\mathbf{x}_{mn}) n_i(\mathbf{x}_m) \right] \quad (l = x, y) \tag{3.6}$$

where $N_{seg}$is the number of segments of the boundary Γ_k, N_{gau} is the number of Gauss points located in each segment on Γ_k, and w_n is the corresponding weight number of Gauss integration scheme. The value of N_{gau} should be determined according to the orders of shape functions.

Then using Eq. (3.3), the smoothed strains corresponding to each edge-based smoothing domain can be obtained.

3.3. *Construction of linear strain field*

The development of W^2 formulation, which seeks solutions form a G space, has discovered a legal way to construct the strain fields more freely, and also provides the possibilities far beyond the standard Galerkin formulations. In the scheme of the NS-, ES- and CS-based methods developed based on the GS-Galerkin weak form, constant strains are constructed over node-based or edge-based smoothing domains, which are stationary, non-overlapping and acting as integration cells. In the scheme of the SC-PIM models which are developed based on the SC-Galerkin weak form, linear strain fields are constructed over each integration cell based on the smoothed strains. Note that the smoothing domains used in the SC-PIM models can be movable, may overlap (or have gap) and do not serve as integration cells.

In this work, the problem domain is first divided into N_{cell} three-node triangular background cells and each of them will be acting as an integration cell, so that $\Omega = \cup_{k=1}^{N_{inte}} \Omega_k = \cup_{k=1}^{N_{cell}} \Omega_k$ and $\Omega_i \cap \Omega_j = \emptyset$, $i \neq j$. Next, by performing the generalized strain smoothing operation over the edge-based smoothing domains, shown in (b) of Fig. 1, the smoothed strains can be obtained corresponding to the edges of triangles using Equation (3.3). In each triangular background cell, four sub-triangles can be further constructed by connecting the three mid-edge points, as illustrated using dotted lines in Fig. 2. We assume that the strain at a vertex is the same as that at the mid-edge-point of the corresponding opposite edge. Clearly the strain fields within each of the four sub-triangle are linear, and the strain values at the three vertexes of a sub-triangle are the same as those of another sub-triangle. Then the strain field within any of the four sub-triangles can be obtained using the

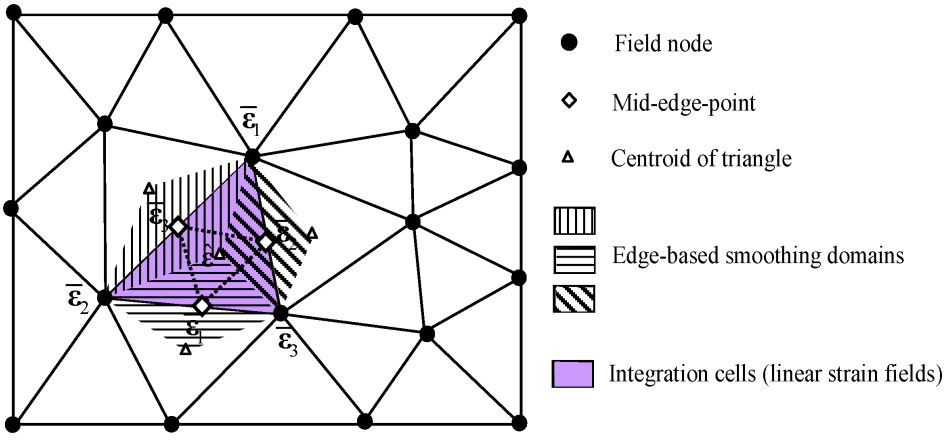

Fig. 2. Piecewisely linear strain field construction: Each triangular background cell is divided into four sub-triangles; The strains at mid-edge-points of the three edges are obtained via the generalized gradient smoothing over the edge-based smoothing domains; The strain at a vertex is assumed to be the mid-edge strain of the opposite edge. The strain field in each sub-triangle is assumed linear.

following linear interpolation:

$$\hat{\boldsymbol{\varepsilon}}(\mathbf{x}) = \sum_{i=1}^{3} \boldsymbol{\Phi}_i(\mathbf{x}) \bar{\boldsymbol{\varepsilon}}_i \tag{3.7}$$

where $\hat{\boldsymbol{\varepsilon}}$ is the vector of constructed linear strains, $\boldsymbol{\Phi}$ is the vector of PIM shape functions and $\bar{\boldsymbol{\varepsilon}}$ is the edge-based smoothed strains corresponding to each edge, which are obtained using Eq. (3.3).

Substituting Eq. (3.3) into Eq. (3.7), the linearly-constructed strain $\hat{\boldsymbol{\varepsilon}}$ within the sub-triangle of integration cell can also be expressed as

$$\hat{\boldsymbol{\varepsilon}}(\mathbf{x}) = \sum_{i=1}^{3} \boldsymbol{\Phi}_i(\mathbf{x}) \bar{\mathbf{B}}_i \mathbf{d}_i = \hat{\mathbf{B}} \mathbf{d} \tag{3.8}$$

in which $\hat{\mathbf{B}} = [\boldsymbol{\Phi}_1 \bar{\mathbf{B}}_1 \quad \boldsymbol{\Phi}_2 \bar{\mathbf{B}}_2 \quad \boldsymbol{\Phi}_3 \bar{\mathbf{B}}_3]$ is the strain matrix corresponding to the linearly-constructed strain $\hat{\boldsymbol{\varepsilon}}$ and $\mathbf{d} = [\mathbf{d}_1 \quad \mathbf{d}_2 \quad \mathbf{d}_3]^{\mathrm{T}}$.

3.4. *Discretized system equations*

After the construction of the displacement and strain fields using Eq. (3.1) and Eq. (3.7) respectively, we need to find out a proper principle to derive the discretized system equations. One option is the modified Hellinger-Reissner variational principle with the assumed strain vector and displacement field as independent field variables (Pian and Wu, 2006). However, the procedure for creating the system equations will be more complicated than the standard FEM using the standard Galerkin weakform. In addition the Hellinger-Reissner variational principle requires the assumed displacement function being continuous. If the assumed displacement function being continuous and the constructed strain field satisfies the orthogonal conditions (Simo and Rifai, 1990), the so-called smoothed Galerkin weakform can be used, as in the ES-FEM (Liu, Nguyen and Lam, 2008) and NS-FEM (Liu and Nguyen *et al.*, 2008) . If the assumed displacement function being discontinuous we need to use the generalized smoothed Galerkin (GS-Galerkin) weakform (Liu, 2008a), as in the ES-PIM (Liu and Zhang, 2008b) and NS-PIM (Liu and Zhang *et al.*, 2005).

Liu (2009) has shown that if the constructed strain field is equivalent to a compatible one in a norm, the so-called strain constructed Galerkin (SC-Galerkin) weakform can be used. Although may not be able to pass the standard patch test, a properly formulated SC-Galerkin model can produce stable and convergent solutions. The equivalence is rather easy to satisfy: the integration cells for strain field construction should not be larger than the cells used for the displacement construction, and the nodal PIM shape functions must be linearly independent and with at least complete linear terms. For the present model, area of the integration cell is 1/4 of that of the displacement construction cell, and thus we use the following SC-Galerkin weak form to create the discretized system equations.

Consider a deformable body occupying domain Ω in motion, subjected to body forces $\mathbf{b}$, external applied traction $\mathbf{t}_\Gamma$ on boundary Γ_t and displacement boundary conditions $\mathbf{u} = \bar{\mathbf{u}}$ on Γ_u. If the inertial and damping forces are also considered in the dynamic equilibrium equations, the SC-Galerkin weak formulation can be presented as (Liu, 2009):

$$\int_\Omega \delta(\hat{\boldsymbol{\varepsilon}}(\mathbf{u}))^T \mathbf{D}(\hat{\boldsymbol{\varepsilon}}(\mathbf{u}))d\Omega - \int_\Omega \delta\mathbf{u}^T[\mathbf{b} - \rho\ddot{\mathbf{u}} - c\dot{\mathbf{u}}]\, d\Omega - \int_{\Gamma_t} \delta\mathbf{u}^T \mathbf{t}_\Gamma d\Gamma = 0 \tag{3.9}$$

It can be found that the above SC-Galerkin weak form has exactly the same form as the standard Galerkin weak form. Therefore, the detailed formulation procedure will be exactly the same as that in the standard FEM and all we need to do is to use the constructed strains $\hat{\varepsilon}$ in place of the compatible strains ε. The overall procedure of the present method is as follows. We first construct the displacement field by linear interpolation using Eq. (3.1), and further obtain the edge-based smoothed strains $\bar{\boldsymbol{\varepsilon}}$ using Eq. (3.3). Next, we construct the linear strain fields using interpolation (Eq. (3.7)) with the edge-based smoothed strains at the mid-edge points of the integration cells. Finally, by substituting the assumed displacements and the constructed strain fields into the Eq. (3.9), and invoking the arbitrary nature of the variation operations, a set of discretized algebraic system equation can be finally obtained in the following matrix form.

$$\mathbf{M}\ddot{\hat{\mathbf{d}}} + \mathbf{C}\dot{\hat{\mathbf{d}}} + \hat{\mathbf{K}}\hat{\mathbf{d}} = \mathbf{f} \tag{3.10}$$

where $\mathbf{M}$ is the mass matrix, $\mathbf{C}$ is the damping matrix and $\mathbf{f}$ is the force vector which are defined as

$$\mathbf{M} = \int_\Omega \rho \boldsymbol{\Phi}^{\mathrm{T}} \boldsymbol{\Phi} d\Omega \tag{3.11}$$

$$\mathbf{C} = \int_\Omega c \boldsymbol{\Phi}^{\mathrm{T}} \boldsymbol{\Phi} d\Omega \tag{3.12}$$

$$\mathbf{f} = -\int_\Omega \boldsymbol{\Phi}^{\mathrm{T}} \mathbf{b} d\Omega + \int_{\Gamma_t} \boldsymbol{\Phi}^{\mathrm{T}} \mathbf{t}_\Gamma d\Gamma \tag{3.13}$$

in which ρ is the mass density and c is the damping parameter.

In Eq. (3.10), the stiffness matrix $\hat{\mathbf{K}}$ is assembled from the sub-stiffness matrix for all the integration cells, which are triangular background cells for the present method.

$$\hat{\boldsymbol{K}}_{ij} = \sum_{k=1}^{N_{inte}} \hat{\boldsymbol{K}}_{ij(k)} = \sum_{k=1}^{N_{cell}} \hat{\boldsymbol{K}}_{ij(k)} \tag{3.14}$$

in which $\hat{\mathbf{K}}_{ij(k)}$ is the sub-stiffness matrix associated with integration cell k which is computed using

$$\hat{\mathbf{K}}_{ij(k)} = \int_{\Omega_k} \hat{\mathbf{B}}_i^T \mathbf{D} \hat{\mathbf{B}}_j d\Omega \tag{3.15}$$

where $\hat{\mathbf{B}}$ is the strain matrix corresponding to the modified strain field $\hat{\varepsilon}$ within the integration cell Ω_k.

In this work, because the strain values at the three vertexes of a sub-triangle are the same as those of other sub-triangles, the four sub-triangles of each background cell should have the same value of strain energy. Therefore, $\hat{\mathbf{K}}_{ij(k)}$ in Eq. (3.15) can be easily calculated using

$$\hat{\mathbf{K}}_{ij(k)} = 4 \int_{\Omega_k^{sub}} \hat{\mathbf{B}}_i^T \mathbf{D} \hat{\mathbf{B}}_j d\Omega \tag{3.16}$$

where Ω_k^{sub} is the area of the central sub-triangle of the integration cell k and $\hat{\mathbf{B}}$ is obtained from Eq. (3.8). Also because the strain fields within each of the four sub-triangles are linear, the above integration can be evaluated analytically using area coordinates, and hence no numerical integration is needed in our SC-PIM.

3.5. *Static, free and forced vibration analysis*

For static problems, the equation can be obtained simply by removing the dynamic terms in Eq. (3.10):

$$\hat{\mathbf{K}}\hat{\mathbf{d}} = \mathbf{f} \tag{3.17}$$

For free vibration analysis, we do not consider the damping and the force terms, and hence Eq. (3.10) reduces to

$$\mathbf{M}\ddot{\hat{\mathbf{d}}} + \hat{\mathbf{K}}\hat{\mathbf{d}} = \mathbf{0} \tag{3.18}$$

A general solution of such an equation can be written as

$$\hat{\mathbf{d}} = \hat{\mathbf{d}}_A \exp(i\omega t) \tag{3.19}$$

where t indicates time, $\hat{\mathbf{d}}_A$ is the amplitude of the nodal displacement or the eigenvector and ω is natural frequency that is found from

$$(-\omega^2 \mathbf{M} + \hat{\mathbf{K}})\hat{\mathbf{d}}_A = \mathbf{0} \tag{3.20}$$

For forced vibration analysis, Eq. (3.10) can be solved by direct integration methods in the same way as in the FEM. For simplicity, the Rayleigh damping is considered in this study, and damping matrix $\mathbf{C}$ is assumed to be a linear combination of $\mathbf{M}$ and $\hat{\mathbf{K}}$,

$$\mathbf{C} = \alpha \mathbf{M} + \beta \hat{\mathbf{K}} \tag{3.21}$$

where α and β are the Rayleigh damping coefficients.

Many direct integration schemes can be used to solve the second-order time dependent problems, such as the Newmark method, Grank-Nicholson method, etc.

In this work, we use the Newmark method to solve the forced vibration problems. When the state at $t = t_0(\hat{\mathbf{d}}_0, \dot{\hat{\mathbf{d}}}_0, \ddot{\hat{\mathbf{d}}}_0)$ is known, we aim to find the new state at $t_1 = t_0 + \theta\Delta t(\hat{\mathbf{d}}_1, \dot{\hat{\mathbf{d}}}_1, \ddot{\hat{\mathbf{d}}}_1)$ where $0.5 \leq \theta \leq 1$, using the following formulations:

$$\left[\left(\alpha + \frac{1}{\theta\Delta t}\right)\mathbf{M} + (\beta + \theta\Delta t)\hat{\mathbf{K}}\right]\hat{\mathbf{d}}_1 = \theta\Delta t\mathbf{f}_1 + (1-\theta)\Delta t\mathbf{f}_0 + \left(\alpha + \frac{1}{\theta\Delta t}\right)\mathbf{M}\hat{\mathbf{d}}_0 + \frac{1}{\theta}\mathbf{M}\dot{\hat{\mathbf{d}}}_0 + [\beta - (1-\theta)]\,\hat{\mathbf{K}}\hat{\mathbf{d}}_0 \tag{3.22}$$

$$\dot{\hat{\mathbf{d}}}_1 = \frac{1}{\theta\Delta t}(\hat{\mathbf{d}}_1 - \hat{\mathbf{d}}_0) - \frac{1-\theta}{\theta}\dot{\hat{\mathbf{d}}}_0 \tag{3.23}$$

$$\ddot{\hat{\mathbf{d}}}_1 = \frac{1}{\theta\Delta t}(\dot{\hat{\mathbf{d}}}_1 - \dot{\hat{\mathbf{d}}}_0) - \frac{1-\theta}{\theta}\ddot{\hat{\mathbf{d}}}_0 \tag{3.24}$$

4. Numerical Examples

Some benchmark numerical examples are studied to investigate the properties of the present method. Two error indicators with respect to displacement and energy are defined as follows:

$$e_d = \sqrt{\frac{\sum_{i=1}^{N_{node}}(u_i^{exact} - u_i^{numerical})^2}{\sum_{i=1}^{N_{node}}(u_i^{exact})^2}} \tag{4.1}$$

$$e_e = \frac{1}{A}\sqrt{\frac{1}{2}\int_\Omega (\varepsilon^{exact} - \varepsilon^{numerical})^{\mathrm{T}}\mathbf{D}(\varepsilon^{exact} - \varepsilon^{numerical})d\Omega} \tag{4.2}$$

where the superscript *exact* denotes the exact or analytical solution, *numerical* denotes a numerical solution obtained using a numerical method including the present SM-PIM, N_{node} is the number of total field nodes and $A$is the area of the problem domain.

4.1. *Standard patch test*

The first case studied is the standard (linear) patch test. Satisfaction of the standard patch test requires that the displacements of all the interior nodes of the patch follow "exactly" (to machine precision) the same linear function of the imposed displacement on the boundary of the patch. For a numerical method working for solid mechanics problems, the sufficient requirement for convergence is to pass the standard patch test (Zienkiewicz and Taylor, 2000). The patch is a unit square domain with 109 irregularly distributed nodes, as shown in Fig. 3, and the displacements

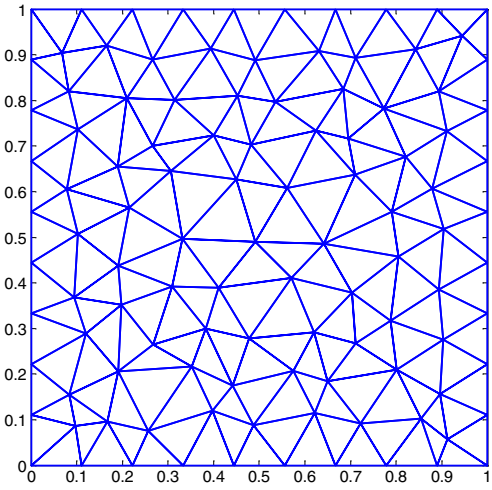

Fig. 3. Domain discretization using three-node triangular cells of unit square with 109 irregularly distributed nodes.

are prescribed on all the boundaries by the following linear functions.

$$\begin{cases} u_x = 0.6x \\ u_y = 0.6y \end{cases} \tag{4.3}$$

The analytical solution for this problem is a linear displacement field given by the above equation over the entire patch. For the present method using T3 and T6/3 schemes, errors of numerical results in displacements norm are $3.227E-15$ and $3.261E-14$ respectively. It clearly showed that the present method can pass the patch test to machine accuracy.

4.2. *A cantilever subjected to parabolic tractions at the free end*

A cantilever with length $L$and height $D$is studied, which is subjected to a parabolic traction on the right edge as shown in Fig. 4. As the cantilever is assumed to have unit thickness, analytical solutions based on the plane stress theory is available

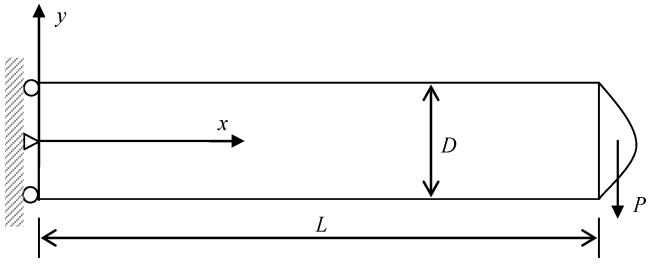

Fig. 4. Rectangular cantilever subjected to a parabolic traction on the right edge.

(Timoshenko and Goodier, 1970):

$$u_x = -\frac{py}{6EI}\left[(6L-3x)x + (2+\nu)(y^2 - \frac{D^2}{4})\right] \tag{4.4}$$

$$u_y = \frac{p}{6EI}\left[3\nu y^2(L-x) + (4+5\nu)\frac{D^2 x}{4} + (3L-x)x^2\right] \tag{4.5}$$

$$\sigma_x = -\frac{p(L-x)y}{I}, \quad \sigma_y = 0, \quad \sigma_{xy} = \frac{p}{2I}\left[\frac{D^2}{4} - y^2\right] \tag{4.6}$$

where I is the moment of the inertia given as$I = D^3/12$. The values of the parameters are taken as: $E = 3.0 \times 10^7\,\text{Pa}$, $v = 0.3$, $L = 50\,\text{m}$, $D = 10\,\text{m}$ and $P = -1000\,\text{N}$.

Using the same set of three-node triangular meshes, shown in Fig. 5, the cantilever is studied using the present method, together with the FEM, linear NS-PIM and linear ES-PIM which use T3 scheme. The FEM is chosen as the "bottom line": the present method should perform as good as the liner FEM, or has some special properties that the linear FEM does not have. The NS-PIM is chosen for comparison, because we know it can give upper bound solutions. The "legend" ES-PIM is chosen because the ES-PIM model has been found to have very close-to-exact stiffness and is known as the "most" accurate linear model among the numerical methods based on W^2 formulation.

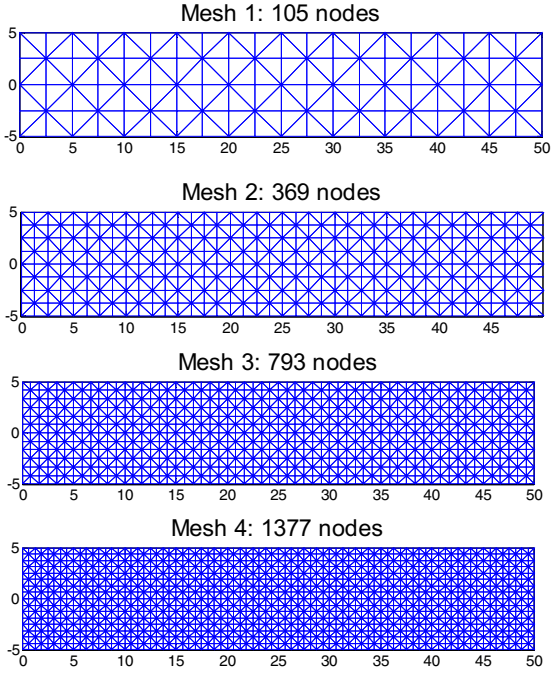

Fig. 5. Domain discretization using three-node triangular cells for the problem of cantilever subjected to a parabolic traction on the right edge.

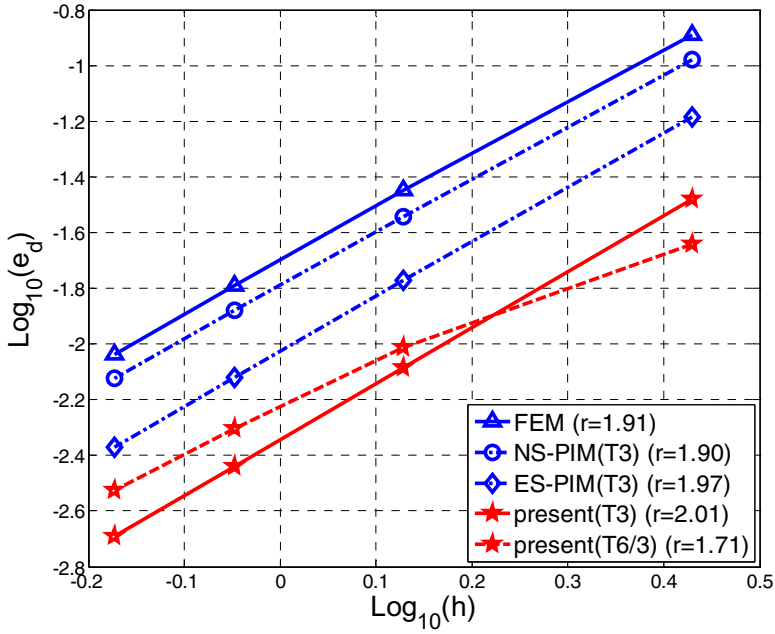

Fig. 6. Convergence of the numerical results in displacement norm for the rectangular cantilever solved using different methods with the same set of triangular mesh.

Figure 6 plots the convergence of the solutions in displacement norm for the cantilever solved using different methods. The solutions of all these methods converge with the reducing nodal spacing at about the similar convergence rate that is close to the theoretical value of 2.0 for both the weak and weakened weak (W^2) formulations (Liu, 2008c). In terms of accuracy, NS-PIM obtains similar results compared with the linear FEM, ES-PIM provides much better results than the FEM and NS-PIM, and the present method performs the best, for both T3 and T6/3 schemes. Figure 7 plots the convergence of the solutions in energy norm for the same cantilever solved using different methods. We found the linear FEM converges at the rate of 0.94, which is very close to the theoretical value of 1.0. ES-PIM and the present method with T3 scheme obtains similar convergence rates but better accuracy compared to the FEM. In terms of both accuracy and convergence, the present method with T6/3 scheme stands out together with the NS-PIM.

Figure 8 plots the process of the strain energies converging to the exact solution for the cantilever beam obtained using different methods. The exact value of strain energy for this problem is 8.593333333, which is calculated by analytical integration using the stresses given in Equation (4.6). As expected, the FEM and NS-PIM give the lower and upper bound solutions respectively, and they also provide the energy bound to the ES-PIM and the proposed method. The present method performs more softly than the ES-PIM and more stiffly than the NS-PIM, and the solutions are

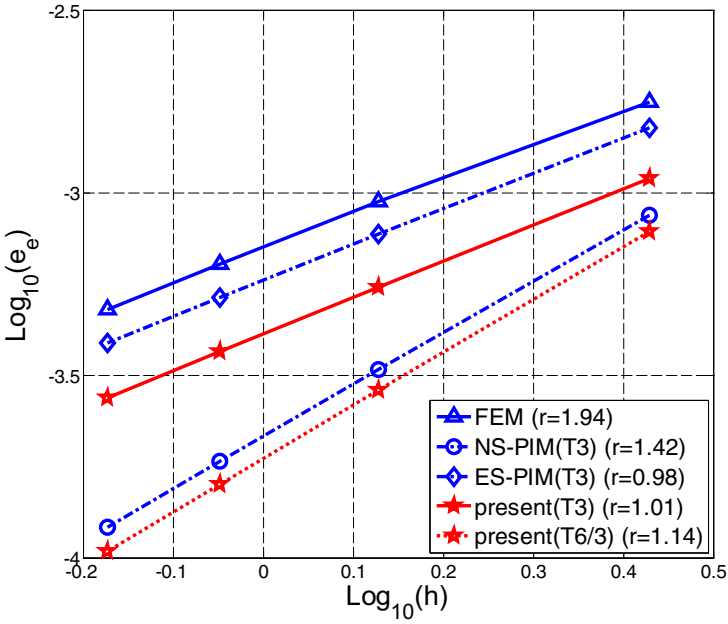

Fig. 7. Convergence of the numerical results in energy norm for the rectangular cantilever solved using different methods with the same set of triangular mesh.

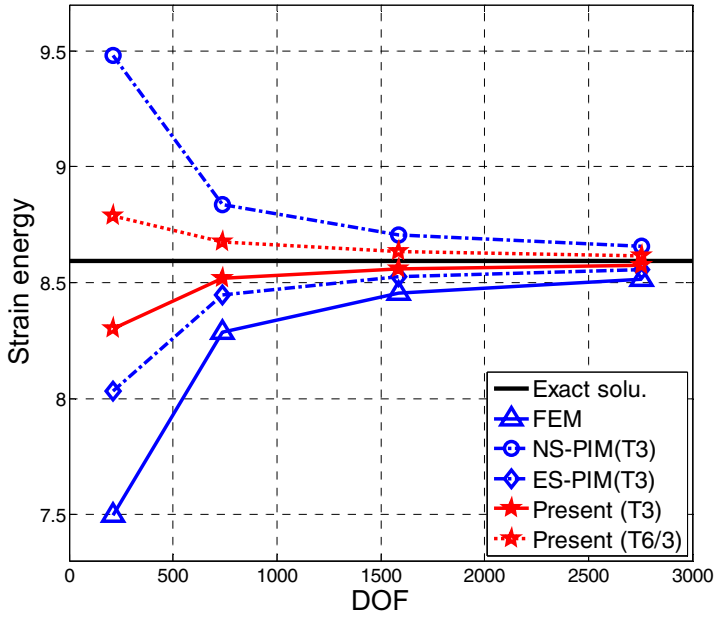

Fig. 8. Solutions in strain energy converging to the exact solution for the rectangular cantilever solved using different methods and same set of triangular mesh.

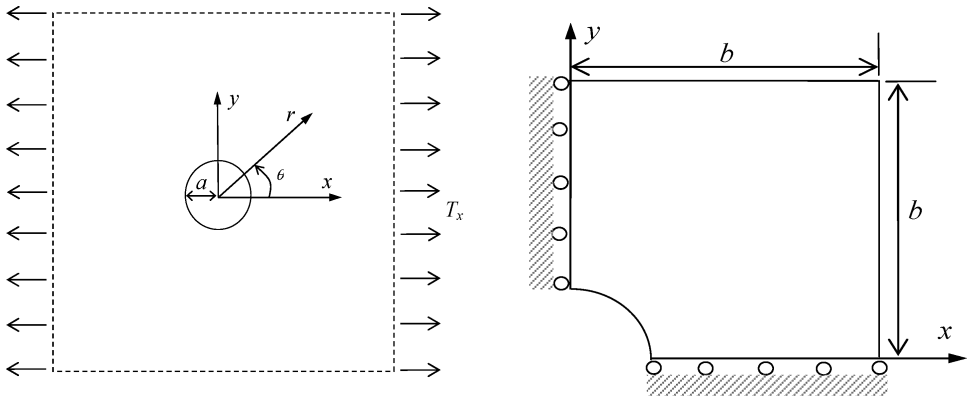

Fig. 9. Infinite plate with a circular hole subjected to uniform tensile and its quadrant model.

bounded by these two methods from lower and upper respectively. It means that the present method possesses an even more close-to-exact stiffness and hence can obtain more accurate results than both NS-PIM and ES-PIM. Between the two schemes of the present method, i.e. T6/3 scheme and T3 scheme, the former behaves more softly than the latter does. As we discussed previously, one issue that affects the softness of the model is the order of shape functions used in the displacement approximation: when higher order shape functions are used, the displacements approximated in a smoothing domain are closer to the exact one, and this will reduce the stiffening effect and vice versa. This explains the phenomena that the present method with T6/3 scheme performs more softly than that with T3 scheme.

4.3. *Infinite plate with a circular hole*

As shown in Fig. 9, an infinite solid with a central circular hole of radius a and subjected to a unidirectional tensile (T_x) is studied. Due to its two-fold symmetry, only one quarter is modeled with the length of b. Thus symmetry conditions are imposed on the left and bottom edges and the inner boundary of the hole is traction free. For this benchmark problem, the analytical solution is available as follows (Timoshenko and Goodier, 1970):

$$u_x = \frac{T_x a}{8\mu}\left[\frac{r}{a}(\kappa+1)\cos\theta + 2\frac{a}{r}((1+\kappa)\cos\theta + \cos(3\theta)) - 2\frac{a^3}{r^3}\cos(3\theta)\right] \quad (4.7)$$

$$u_y = \frac{T_x a}{8\mu}\left[\frac{r}{a}(\kappa-3)\sin\theta + 2\frac{a}{r}((1-\kappa)\sin\theta + \sin(3\theta)) - 2\frac{a^3}{r^3}\sin(3\theta)\right] \quad (4.8)$$

$$\sigma_{xx} = T_x\left\{1 - \frac{a^2}{r^2}\left[\frac{3}{2}\cos(2\theta) + \cos(4\theta)\right] + \frac{3a^4}{2r^4}\cos(4\theta)\right\} \quad (4.9)$$

$$\sigma_{yy} = -T_x \left\{ \frac{a^2}{r^2} \left[\frac{1}{2}\cos(2\theta) - \cos(4\theta) \right] + \frac{3a^4}{2r^4}\cos(4\theta) \right\} \tag{4.10}$$

$$\sigma_{xy} = -T_x \left\{ \frac{a^2}{r^2} \left[\frac{1}{2}\sin(2\theta) + \sin(4\theta) \right] - \frac{3a^4}{2r^4}\sin(4\theta) \right\} \tag{4.11}$$

where μ is the shear modulus and κ is the Kolosov which are defined as

$$\mu = \frac{E}{2(1+v)}, \quad \kappa = \begin{cases} 3-4v & \text{(Plane strain)} \\ \dfrac{3-v}{1+v} & \text{(Plane stress)} \end{cases} \tag{4.12}$$

In the above equations, $(r,\ \theta)$ are the polar coordinates and θ is measured counterclockwise from the positive x-axis. The values of the parameters are taken as: $E = 3.0 \times 10^7\,\text{Pa}$, $v = 0.3$, $a = 1\,\text{m}$, $b = 5\,\text{m}$ and $T_x = 10\,\text{N/m}$. The problem is studied as a plane stress problem and traction boundary conditions are imposed on the right and upper edges with the exact stresses obtained using Eqs. (4.9)–(4.11).

Using the same set of triangular meshes, shown in Fig. 10, this problem is studied using the present method, together with the standard FEM, NS-PIM(T3) and ES-PIM(T3). Fig. 11 plots the convergence of the solutions in displacement norm for this problem solved using different methods. The NS-PIM obtains similar results as the standard FEM. Results of the ES-PIM are of higher convergence rate and better accuracy than both FEM and NS-PIM. In terms of accuracy and convergence, the present method using T3 scheme performs the best, in which the accuracy is about 10 times more accurate than the linear FEM. Figure 12 plots the convergence of

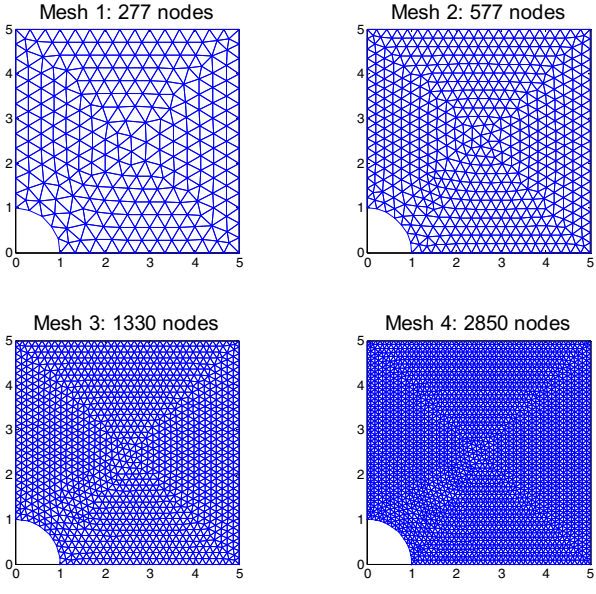

Fig. 10. Domain discretization using three-node triangular cells for the problem of infinite plate with a circular hole subjected to uniform tensile.

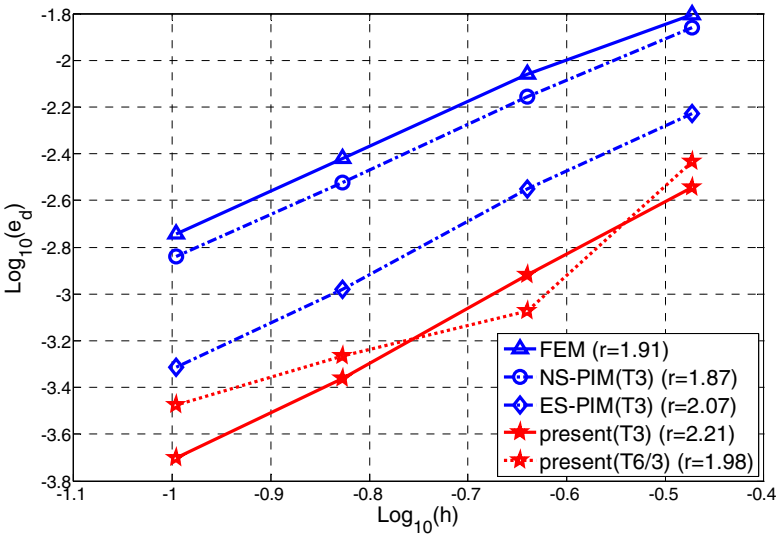

Fig. 11. Convergence of the numerical results in displacement norm for the problem of infinite plate with a hole solved using different methods with the same set of triangular mesh.

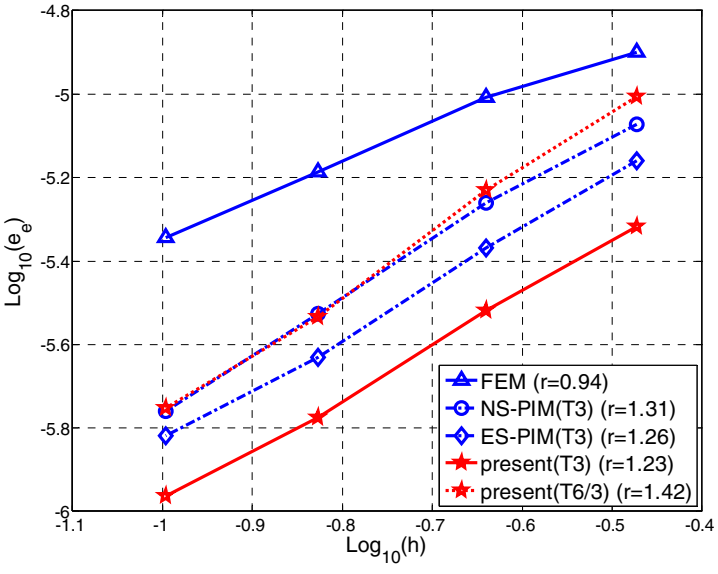

Fig. 12. Convergence of the numerical results in energy norm for the problem of infinite plate with a hole solved using different methods with the same set of triangular mesh.

the solutions in energy norm for the present case solved using different methods. All the methods based on W^2 formulations, including NS-PIM, ES-PIM and the present method, perform better than the linear FEM in terms of both accuracy and convergence. Among all the methods, the present method with T3 scheme stands out.

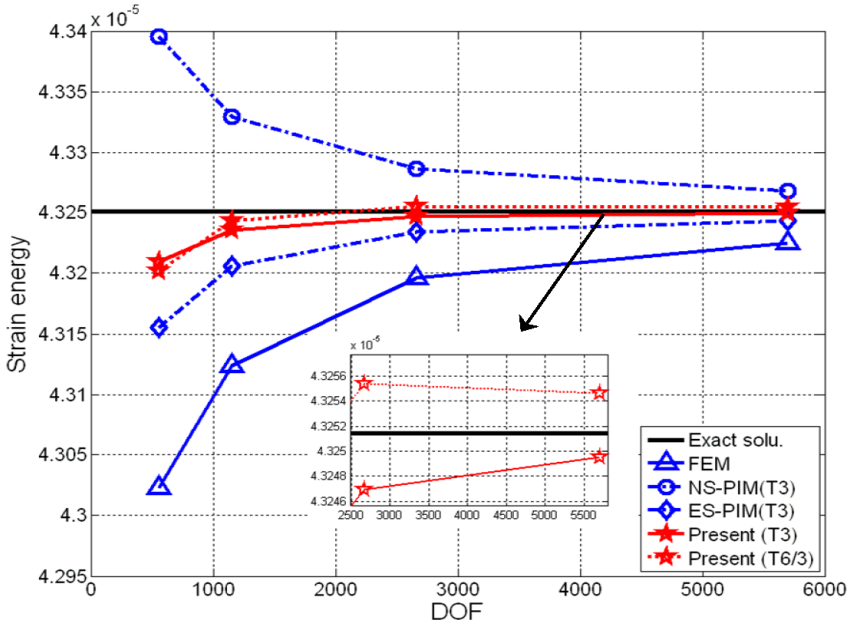

Fig. 13. Solutions in strain energy converging to the exact solution for the problem of infinite plate with a hole solved using different methods and same set of triangular mesh.

Figure 13 plots the strain energies converging to the exact solution for the problem of infinite solid with a hole obtained using different methods, in which the exact strain energy is calculated using the stresses given in Eqs. (4.9)–(4.11) by analytical integration and the value is 4.325139892E-5. Again we found that the FEM and NS-PIM give lower and upper bound solutions respectively. Solutions of the ES-PIM are bounded by those of the FEM and NS-PIM and converge to the reference solutions from below. The results of the present method are bounded by the ES-PIM and NS-PIM from lower and upper respectively, which means that the present method behaves more softly than the ES-PIM and more stiffly than the NS-PIM, and can obtain more accurate results than the others. Same as the previous case, the present method with T6/3 scheme performs more softly than that with T3 scheme, when the problem is discretized using more background cells. Note that when more nodes are used to present the problem domain, solution of the present method with T6/3 scheme may cross the exact value of the strain energy and converge to it from above with further increasing of the DOF.

4.4. *Automotive part: Rim*

A typical rim of automotive component is studied using the present method. As shown in Fig. 14, the rim is restricted along the inner circle and a uniform pressure of 100 units is applied along the outer arc edge of 60°. The parameters are taken

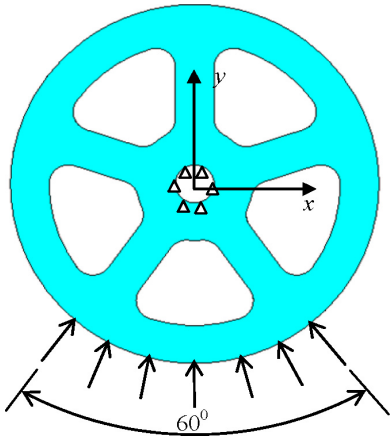

Fig. 14. Model of an automotive rim.

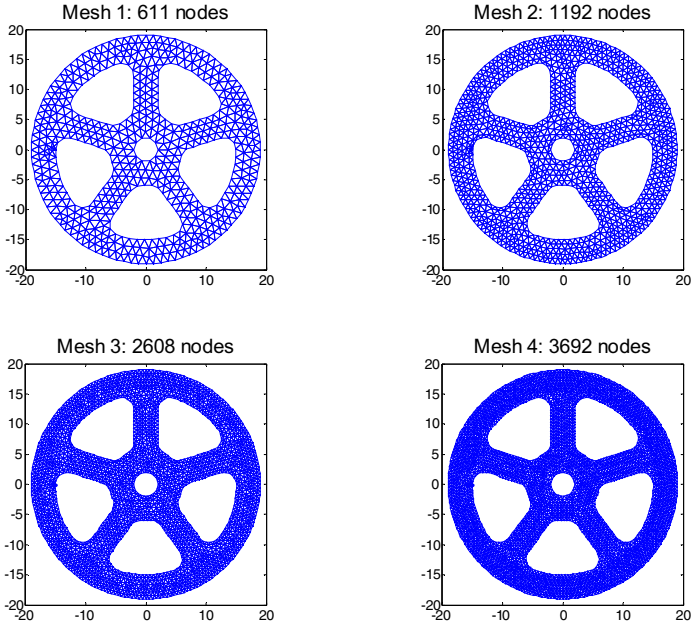

Fig. 15. Domain discretization using three-node triangular cells for the problem of automotive rim.

as: $E = 3.0 \times 10^7\,\text{Pa}$ and $v = 0.3$. The rim is studied as a plane stress problem using various numerical methods with the same set of triangular elements as shown in Fig. 15.

Figure 16 plots the strain energies converging to the reference solution for the rim problem obtained using different methods. As no analytical solutions available

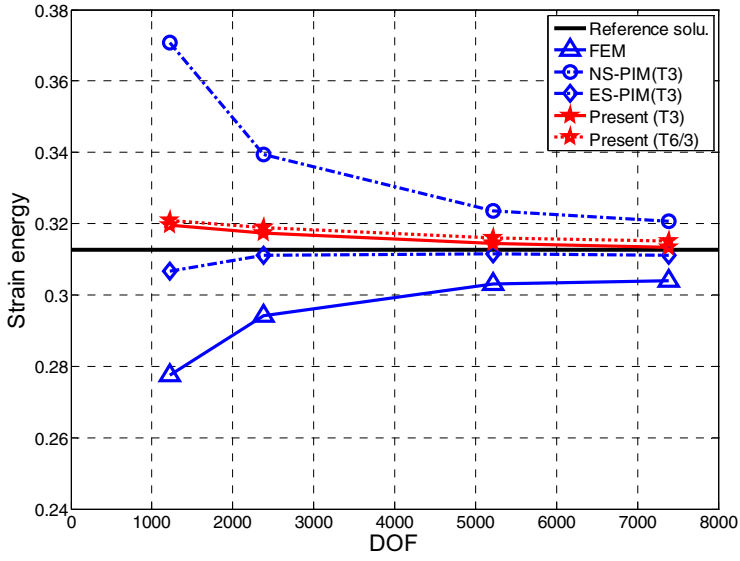

Fig. 16. Solutions in strain energy converging to the exact solution for the problem of automotive rim solved using different methods and same set of triangular mesh.

for this problem, a reference value of the strain energy has been obtained using the standard FEM with a very fine mesh (total 14332 nodes). For this problem with complicated shape, the FEM and NS-PIM give lower and upper bound solutions respectively, which bound the exact one as well as those obtained using other numerical methods. Solutions of the ES-PIM are very close to the reference one and convergence to it from below. The present method performs more softly than the overly-stiff FEM and more stiffly than the overly-soft NS-PIM. Solutions of the present method are also very close to the reference one and convergence to it from above with the increasing of DOF. Same as the previous cases, we found that the present method with T6/3 scheme performs more softly than that with T3 scheme, which is consistent with the discussion in the earlier work (Liu and Zhang, 2008a).

4.5. *Free vibration analysis of a slender rectangular cantilever*

In this example, free vibration analysis is performed for a slender cantilever beam with $L = 100\,\text{mm}$, $D = 10\,\text{mm}$, thickness $t = 1.0\,\text{mm}$, Young's modulus $E = 2.1\times10^4\,\text{kgf/mm}^4$, Poisson's ratio $v = 0.3$, mass density $\rho = 8.0\times10^{-10}\,\text{kgf s}^2/\text{mm}^4$. A plane stress problem is considered. Because the slenderness of the beam, the Euler-Bernoulli beam theory is used to obtain the fundamental frequency $f_1 = 0.08276 \times 10^4\,\text{Hz}$ as a reference. Three regular meshes are used in the analysis. Numerical results using the FEM of four node quadrangular elements (FEM-Q4) with a very fine mesh (100×10) for the same problem are computed and used as reference solutions.

Table 1. First twelve natural frequencies (in 10kHz) of the slender cantilever.

Model	Present (T3)	ES-PIM (T3)	FEM (T3)	Reference solu.
Mesh: 10×1	0.0761	0.1048	0.1692	0.0824
Nodes: 22	0.4471	0.6018	0.9163	0.4944
Background cells:	1.1591	1.2833	1.2869	1.2824
Three-node triangular cell	1.2823	1.5177	2.1843	1.3022
	2.0790	2.6362	3.5942	2.3663
	3.1239	3.7724	3.8338	3.6085
	3.7647	3.8559	5.0335	3.8442
	4.2072	5.0349	6.2421	4.9674
	5.2348	6.0827	6.4154	6.3960
	5.9901	6.1520	7.5940	6.4023
	6.1245	7.0519	8.4790	7.8853
	6.7230	7.7212	8.7033	8.9290
Mesh: 20×2	0.0786	0.0853	0.1117	0.0824
Nodes: 63	0.4691	0.5078	0.6539	0.4944
Background cells:	1.2257	1.2828	1.2843	1.2824
Three-node triangular cell	1.2824	1.3246	1.6748	1.3022
	2.2021	2.3783	2.9554	2.3663
	3.3086	3.5784	3.8424	3.6085
	3.8235	3.8298	4.3866	3.8442
	4.4724	4.8533	5.8836	4.9674
	5.6418	6.1527	6.3751	6.3960
	6.2939	6.3182	7.4046	6.4023
	6.7832	7.4419	8.8210	7.8853
	7.8733	8.6776	8.9411	8.9290
Mesh: 40×4	0.0812	0.0827	0.0906	0.0824
Nodes: 205	0.4860	0.4950	0.5409	0.4944
Background cells:	1.2765	1.2826	1.2831	1.2824
Three-node triangular cell	1.2825	1.3006	1.4161	1.3022
	2.3106	2.3554	2.5570	2.3663
	3.5062	3.5778	3.8433	3.6085
	3.8392	3.8408	3.8786	3.8442
	4.7981	4.9029	5.3087	4.9674
	6.1410	6.2867	6.3935	6.3960
	6.3712	6.3774	6.8093	6.4023
	7.5031	7.6987	8.3473	7.8853
	8.8567	8.8751	8.9183	8.9290

Table 1 lists the first twelve natural frequencies of the cantilever solved using different methods and the first twelve corresponding vibration modes obtained using the present method with T3 scheme are plotted in Fig. 17. It is observed that the present method does not have any spurious modes. Furthermore, the natural frequencies obtained using the present method are much smaller that those of FEM and ES-PIM, which also explains that the present method performs more softly than both FEM and ES-PIM. The convergence of the present method has also been demonstrated in this table. With the increase of background cells, natural frequencies of this problem obtained using the present method converge to the references ones rapidly.

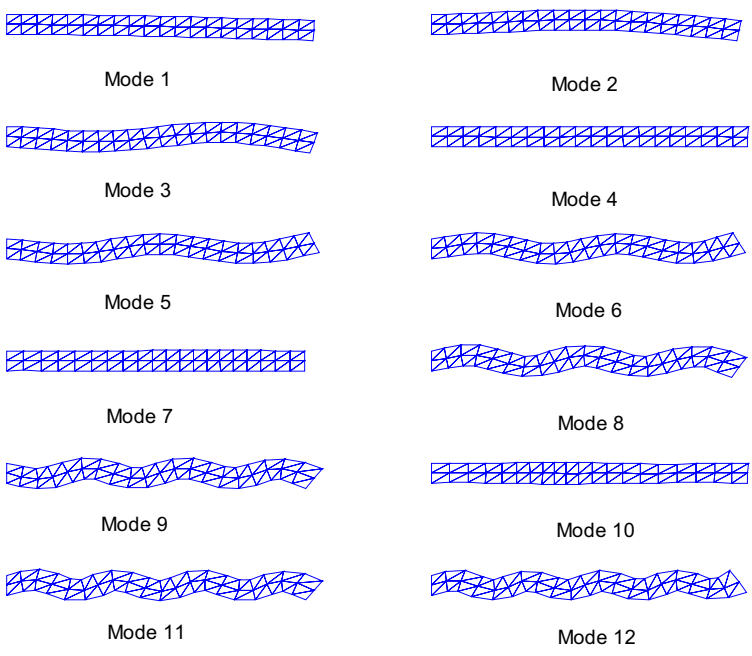

Fig. 17. First 12 free vibration modes of the slender cantilever by the present method with T3 scheme.

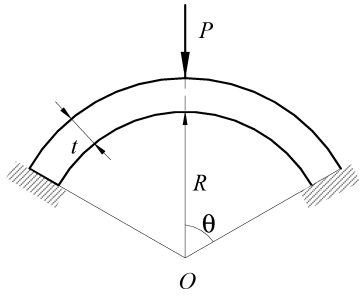

Fig. 18. A spherical shell subjected to point loading at the apex.

4.6. *Forced vibration analysis of a spherical shell*

A spherical shell shown in Fig. 18 is finally now studied. The shell is subjected to a concentrated loading at its apex, and is modeled as 2D solid. A half of the shell is modeled using triangular meshes. The non-dimensional parameters used in the computation are $R = 12$, $t = 0.1$, $\phi = 10.9°$, $\theta = 0.5$, $E = 1.0$, $\nu = 0.3$, and $\rho = 1.0$.

First the problem is studied by subjected to a harmonic loading of $f(t) = \cos \omega_f t$, and the time history of the deflection at the apex of the shell is plotted in Fig. 19 with $\omega_f = 0.05$ and $\Delta t = 5$. It is found all these three methods give nearly identical vibration frequency. The solution of the present method is comparable to that of the

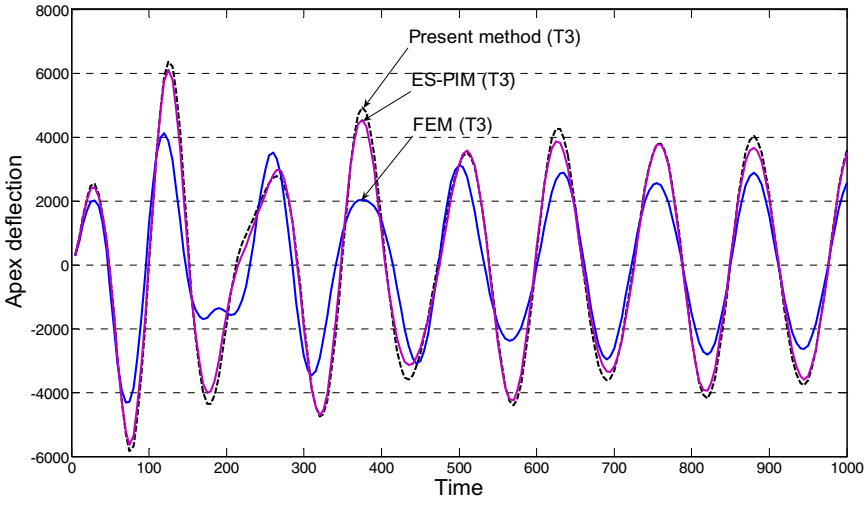

Fig. 19. Solutions of transient responses of the spherical shell subjected to a harmonic loading using different methods.

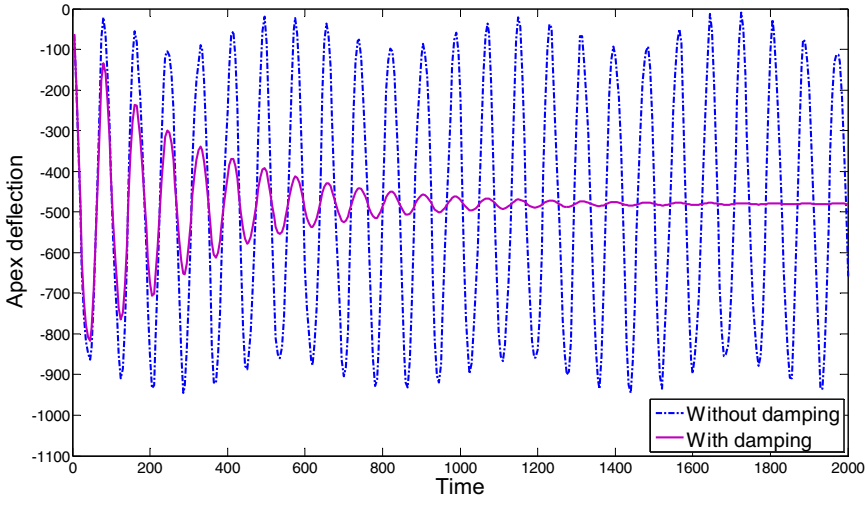

Fig. 20. Solutions of transient responses of the spherical shell subjected to a constant step loading using the present method with T3 scheme.

ES-PIM, and much more accurate than that of the FEM. This may be partially due to the fact both the ES-PIM and the present methods have close-to-exact stiffness. Then the shell excited by a constant step load $f(t) = 1$ starting from $t = 0$ is studied and the response is plotted in Fig. 20. The dash line is for the results without damping, and it is seen that the amplitude of the deflection tends to a

constant value with increasing time. When a Rayleigh damping of $\alpha = 0.005$ and $\beta = 0.272$ are considered, the response convergences to constant quickly.

5. Conclusions

In this work, a novel scheme of strain-constructed point interpolation method (SC-PIM) is formulated, in which the displacement fields are approximated using the PIM shape functions and piecewisely linear strain fields are constructed using the edge-based smoothed strain over each background triangular cell. The SC-Galerkin weak form is used to derive the discretized system equations. A number of numerical examples, including static, free and forced vibration analysis, have been studied using the present method and following conclusions can be drawn:

- The present SC-PIM uses the simplest triangular mesh and no additional degrees of freedom and parameters are introduced, the present method is easy to implement.
- The present method is at least linearly conforming.
- The present model possesses a close-to-exact stiffness: it is more stiff than the "overly-soft" node-based point interpolation method (NS-PIM) and more soft than the "overly-stiff" FEM model.
- For static problems, results of the present method are of superconvergence and ultra-accuracy, and about one order of magnitude more than those of the linear FEM.
- For dynamic problems, there are no spurious non-zeros energy modes found and it is temporally stable, hence the present method works well for dynamic problems.

References

Chen, J. S., Wu, C. T., Yoon, S. and You, Y. [2001] "A stabilized conforming nodal integration for Galerkin mesh-free methods," *International Journal for Numerical Methods in Engineering* **50**, 435–466.

Liu, G. R. [2008a] "A generalized Gradient smoothing technique and the smoothed bilinear form for Galerkin formulation of a wide class of computational methods," *International Journal of Computational Methods* **5**(2), 199–236.

Liu, G. R. [2008b] "A weakened weak (W^2) form for a unified formulation of compatible and incompatible displacement methods," *International Journal for Numerical Methods in Engineering* (revised).

Liu, G. R. [2008c] "On the rate of convergence of weakened weak (W^2) formulations," *International Journal for Numerical Methods in Engineering* (submitted).

Liu, G. R. [2009] *Meshfree Methods: Moving Beyond the Finite Element Method*, 2nd edn. (CRC Press, Boca Raton, USA).

Liu, G. R., Dai, K. Y. and Nguyen, T. T. [2007] "A smoothed finite element method for mechanics problems," *Computational Mechanics* **39**, 859–877.

Liu, G. R., Nguyen, T. T., Dai, K. Y. and Lam, K. Y. [2007] "Theoretical aspects of the smoothed finite element method (SFEM)," *International Journal for Numerical Methods in Engineering* **71**, 902–930.

Liu, G. R., Nguyen, T. T. and Lam, K. Y. [2008] "An edge-based smoothed finite element method (ES-FEM) for static and dynamic problems of solid mechanics," *Journal of Sound and Vibration*, published on line, DOI: 10.1016/j.jsv.2008.08.027.

Liu, G. R., Nguyen, T. T., Nguyen, X. H. and Lam, K. Y. [2008] "A node-based smoothed finite element method (NS-FEM) for upper bound solutions to solid mechanics problems," *Computers and Structures*, published on line, DOI:10.1016/j.compstruc.2008.09.003.

Liu, G. R. and Quek, S. S. [2003] *Finite Element Method: A Practical Course* (Butterworth-heinemann, Burlington, MA).

Liu, G. R., Xu X, Zhang, G. Y. and Gu, Y. T. [2009] "An extended Galerkin weak form and a point interpolation method with continuous strain field and superconvergence using triangular mesh," *Computational Mechanics* **43**, 651–673.

Liu, G. R. and Zhang, G. Y. [2008a] "Upper bound solution to elasticity problems: A unique property of the linearly conforming point interpolation method (LC-PIM)," *International Journal for Numerical Methods in Engineering* **74**, 1128–1161.

Liu, G. R. and Zhang, G. Y. [2008b] "Edge-based smoothed point interpolation methods," *International Journal of Computational Methods* **5**(4), 621–646.

Liu, G. R. and Zhang, G. Y. [2008c] "A strain-constructed point interpolation method (SC-PIM) and strain field construction schemes for mechanics problems of solids and structures using triangular mesh," *International Journal of Solids and Structures* (submitted).

Liu, G. R. and Zhang, G. Y. [2009] "A normed G space and weakened weak (W^2) formulation of a cell-based smoothed point interpolation method," *International Journal of Computational Methods* (accepted).

Liu, G. R., Zhang, G. Y., Dai, K. Y., Wang, Y. Y., Zhong, Z. H., Li, G. Y. and Han, X. [2005] "A linearly conforming point interpolation method (LC-PIM) for 2D mechanics problems," *International Journal of Computational Methods* **2**(4), 645–665.

Nguyen, T. T., Liu, G. R., Lam, K. Y. and Zhang, G. Y. [2008] "A face-based smoothed finite element method (FS-FEM) for 3D linear and nonlinear solid mechanics problems using 4-node tetrahedral elements," *International Journal for Numerical Methods in Engineering*, published on line, DOI: 10.1002/nme.2491.

Pian T. H. H. and Wu, C. C. [2006] *Hybrid and Incompatible Finite Element Methods* (CRC Press, Boca Raton).

Simo, J. C. and Rifai, M. S. [1990] "A class of mixed assumed strain methods and the method of incompatible modes," *International Journal for Numerical Methods in Engineering* **29**, 1595–1638.

Timoshenko, S. P. and Goodier, J. N. [1970] *Theory of Elasticity* (3rd edn). (McGraw-Hill: New York).

Zhang, G. Y., Liu, G. R. and Li, Y. [2008] "An efficient adaptive analysis procedure for certified solutions with exact bounds of strain energy for elasticity problems," *Finite Elements in Analysis and Design* **44**, 831–841.

Zhang, G. Y., Liu, G. R., Wang, Y. Y., Huang, H. T., Zhong, Z. H., Li, G. Y. and Han, X. [2007] "A linearly conforming point interpolation method (LC-PIM) for three-dimensional elasticity problems," *International Journal for Numerical Methods in Engineering* **72**, 1524–1543.

Zienkiewicz, O. C. and Taylor, R. L. [2000] *The Finite Element Method* 5th edn. (Butterworth Heinemann, Oxford, UK).